ROM SAF Report 43
Ref: SAF/ROM/METO/REP/RSR/043
Web: http://rom-saf.eumetsat.int
Date: 11 July 2023

EUMETSAT
ROM SAF
RADIO OCCULTATION METEOROLOGY

ROM SAF Report 43

Applying the ROPP ionospheric 1D-Var retrieval to Metop extension data

Sean Healy

ECMWF

Document Author Table

	Name	***Function***	***Date***
Prepared by:	S. Healy	ROM SAF Project Team	11 July 2023
Reviewed by:	I Culverwell	Met Office	5 May, 2023
Reviewed by:	-	-	-
Approved by:	K. B. Lauritsen	ROM SAF Project Manager	11 July 2023

Document Change Record

Issue/Revision	***Date***	***By***	***Description***
0.1	29 April 2023	S. Healy	First version for review
0.2	26 May 2023	S. Healy	Updates based on review
1.0	11 July 2023	S. Healy	Final Version

ROM SAF

The Radio Occultation Meteorology Satellite Application Facility (ROM SAF) is a decentralised processing centre under EUMETSAT which is responsible for operational processing of GRAS radio occultation (RO) data from the Metop and Metop-SG satellites and radio occultation data from other missions. The ROM SAF delivers bending angle, refractivity, temperature, pressure, humidity, and other geophysical variables in near real-time for NWP users, as well as reprocessed Climate Data Records (CDRs) and Interim Climate Data Records (ICDRs) for users requiring a higher degree of homogeneity of the RO data sets. The CDRs and ICDRs are further processed into globally gridded monthly-mean data for use in climate monitoring and climate science applications.

The ROM SAF also maintains the Radio Occultation Processing Package (ROPP) which contains software modules that aid users wishing to process, quality-control and assimilate radio occultation data from any radio occultation mission into NWP and other models.

The ROM SAF Leading Entity is the Danish Meteorological Institute (DMI), with Cooperating Entities: i) European Centre for Medium-Range Weather Forecasts (ECMWF) in Reading, United Kingdom, ii) Institut D'Estudis Espacials de Catalunya (IEEC) in Barcelona, Spain, and iii) Met Office in Exeter, United Kingdom. To get access to our products or to read more about the ROM SAF please go to: https://rom-saf.eumetsat.int

Intellectual Property Rights

All intellectual property rights of the ROM SAF products belong to EUMETSAT. The use of these products is granted to every interested user, free of charge. If you wish to use these products, EUMETSAT's copyright credit must be shown by displaying the words "copyright (year) EUMETSAT" on each of the products used.

Abstract

A one-dimensional variational (1D-Var) retrieval approach for ionospheric GNSS radio occultation (GNSS-RO) measurements is now included in version 11 of the Radio Occultation Processing Package (ROPP-11: see https://rom-saf.eumetsat.int/ropp/). This 1D-Var code is applied to Metop extension data, where the bending angles extend up to 600 km. It is shown that the 1D-Var code can process the Metop data, but around 15 % of the retrievals either converge to a high cost at convergence value, or fail to converge in 50 iterations. Various problematic cases are presented. Missing bending angles and inconsistent bending angles at the L1 and L2 frequencies can cause retrieval problems. In some cases, the retrieval produces ionospheric layers peaking well below 100 km. A number of additional quality control (QC) checks are suggested. It is found that single frequency retrievals can be performed with simple source code changes.

Contents

1 Introduction **5**

2 Method **6**
2.1 Variational Retrieval 6
2.2 Forward model 6

3 1D-Var retrieval set up and Metop observations **8**

4 Results **9**

5 Summary **17**

1 Introduction

The radio occultation instrument on EUMETSAT's Metop Second Generation (Metop-SG) satellites will measure to around 600 km above the Earth's surface, and provide information for ionospheric and space weather applications. The ROM SAF has developed an ionospheric one dimensional variational (1D-Var) retrieval approach for the truncated Metop-SG measurement geometry. This geometry complicates the application of standard Abel transform retrieval techniques. The new 1D-Var retrieval method is described in more detail by Healy and Culverwell (2021), where it has been tested with COSMIC measurements. In addition, a statistical analysis of 1D-Var results is given by Elvidge (2021), including retrieval comparisons statistics with ionosondes. This report is an extension of these studies, but now applying the 1D-Var to Metop test data sets in preparation for Metop-SG.

The ionospheric 1D-Var code is now available as part of version 11 of the ROM SAF's Radio Occultation Processing Package (ROPP-11: see https://rom-saf.eumetsat.int/ropp/). This code has already been used in the EUMETSAT "GIMA" Project (Hoque *et al.*, 2023), for the assessment of ionospheric information provided in the Metop extension test data sets. However, the ROPP-11 code represents the first implementation of a new approach for the ionospheric retrieval problem, and it was always expected that improvements would be introduced in later ROPP versions, as the observation characteristics and 1D-Var performance were better understood. Therefore, in this work we also use the ROPP-11 1D-Var code to process ionospheric profiles from the Metop extension data, but with the aim of highlighting problematic cases and suggesting possible code improvements. It is demonstrated that the 1D-Var code in ROPP-11 can already successfully process most of the cases, but we show that fairly straightforward quality control (QC) changes can screen out and improve some problematic retrieval cases. We also demonstrate that single frequency 1D-Var retrievals can be performed with quite minor ROPP-11 source code changes.

In Section 2, we briefly review the key aspects of the retrieval approach, noting that more detail is given in Healy and Culverwell (2021). The 1D-Var setup and Metop extension data is described in Section 3. The main results are presented in Section 4, where we give an overview of the retrieval performance, and present a selection of difficult cases that point to possible code improvements. A summary is given in Section 5.

2 Method

2.1 Variational Retrieval

The one-dimensional variational (1D-Var) retrieval approach (e.g., Rodgers 2000) involves adjusting a state vector, $\mathbf{x}$, in order minimise a cost function of the form,

$$J(\mathbf{x}) = \frac{1}{2}(\mathbf{x}-\mathbf{x}_b)^{\mathbf{T}}\mathbf{B}^{-1}(\mathbf{x}-\mathbf{x}_b) + \frac{1}{2}(\mathbf{y}-H(\mathbf{x}))^{\mathbf{T}}\mathbf{R}^{-1}(\mathbf{y}-H(\mathbf{x})) \tag{2.1}$$

where,

- $\mathbf{x}_b$ is the *a priori* estimate of the state
- $\mathbf{y}$ is the vector of observations
- H is the forward operator, mapping parameters in $\mathbf{x}$ to the observation space
- and $\mathbf{B}$ and $\mathbf{R}$ are the *a priori* and observation error covariance matrices, respectively.

In ROPP-11 the ionospheric 1D-Var the state vector, $\mathbf{x}$, is composed of multiple "VaryChap layers". Each VaryChap layer is defined by four parameters:

- Peak electron density: n_m
- Height of peak electron density: r_m
- Scale height parameter at peak electron density: H_m
- Gradient of scale height with height: k.

2.2 Forward model

The electron density n_e at radius r for each VaryChap layer can be written as (Nsumei *et al.* 2012),

$$n_e(r) = n_m\sqrt{\frac{H_m}{H(r)}}\exp\left(\frac{1}{2}(1-u(r)-\exp(-u(r)))\right) \tag{2.2}$$

where for $(r < r_m)$,

$$\begin{aligned} H(r) &= H_m \\ u(r) &= (r-r_m)/H_m \end{aligned} \tag{2.3}$$

and for $(r \geq r_m)$,

$$\begin{aligned} H(r) &= H_m + k(r-r_m) \\ u(r) &= \frac{1}{k}\ln\left(\frac{H(r)}{H_m}\right). \end{aligned} \tag{2.4}$$

Given bending angles at two frequencies ($f_1 = 1575.42$ MHz, $f_2 = 1227.60$ MHz), denoted by α_1 and α_2, respectively, the bending angle forward model, $H(\mathbf{x})$, computes

$$\alpha_2(a) - \alpha_1(a) = k_4\left(\frac{f_1^2 - f_2^2}{f_1^2 f_2^2}\right)\left[a\left[\int_a^{r_L} + \int_a^{r_G}\right]\frac{\frac{dn_e(r)}{dr}}{\sqrt{(r^2-a^2)}}dr - \frac{n_e(r_L)a}{\sqrt{(r_L^2-a^2)}}\right] \tag{2.5}$$

where both the electron density and electron density gradients are determined by the VaryChap parameters given in $\mathbf{x}$, a is the impact parameter of the observation, r_L is the radius of the LEO satellite, r_G is the radius of the GNSS satellite and $k_4 = 40.3\ \mathrm{m}^{-3}\mathrm{s}^{-2}$. This is a one-dimensional approximation of the ionospheric bending problem, which ignores horizontal refractive index gradients and is linear in electron density. We assume a straight line path between the satellites and the impact parameter, a, determines the ray tangent height. This approximation is usually accurate to within 600 m even at electron densities of $3 \times 10^{12}\mathrm{m}^{-3}$ which would occur near 300 km. See Healy and Culverwell (2021) for more details on the derivation of Eq. 2.5.

3 1D-Var retrieval set up and Metop observations

Layer number	Variable(unit)	Value	Uncertainty (σ_b)
1	n_m (m^{-3})	2.0e12	7.5e11
1	$r_m - R_c$ (m)	3.0e5	1.5e5
1	H_m(m)	5.0e4	2.5e4
1	k (m/m)	0.15	0.05
2	n_m (m^{-3})	5.0e11	2.5e11
2	$r_m - R_c$ (m)	1.7e5	5.0e4
2	H_m (m)	3.0e4	2.0e4
2	k (m/m)	0.075	0.025

Table 3.1: The background state and uncertainty information used in the two layer ROPP 1D-Var computations. R_c is the radius of curvature provided with the observation.

The 1D-Var calculations presented here assume two VaryChap layers so we retrieve 8 parameters. The eight *a priori* parameters and assumed uncertainty estimates (standard deviations) are shown in Table 3.1. The $\mathbf{B}$ matrix is assumed to be diagonal. As discussed in Healy and Culverwell (2021), the two layer retrieval problem is well-posed and the *a priori* information is not a strong constraint on the final solution and so it can be effectively viewed as a starting point for the 1D-Var iterations.

The Metop extension data consists of 510 occultations measured on August 1, 2020. The L1 and L2 ionospheric bending angles are processed with the geometrical optics method, and for all occultations they are provided on the same impact heights, between 85 km and 590 km, with a 1 km impact height separation. However, only bending angles in the interval between 150 km and 500 km are used (they are "active") in the 1D-Var retrieval to influence the final state. Therefore, the observation vector, $\mathbf{y}$, is usually composed of 351 $\alpha_2(a) - \alpha_1(a)$ bending angle differences on the 1 km vertical grid between 150 km and 500 km. The standard deviation of the observation errors is assumed to be 2 microradians for all profiles.

4 Results

Figure 4.1 shows twice the 1D-Var cost function values at convergence, divided by the number of observations ($2J/m$) for the Metop measurements. Ideally, these values should be of order 1 if the assumed error statistics used in the 1D-Var are realistic, and the solution has converged correctly (e.g., Rodgers, 2000). However, in this case the mean value of $2J/m$ averaged over all the retrievals is 7.9, and in 69 cases the $2J/m > 10$, with the largest being 882. The number of iterations required for convergence is also useful for identifying difficult cases (Figure 4.2). Nine cases require 40 or more iterations. Overall, around 15 $\%$ of the Metop retrievals are considered problematic based on these two diagnostics.

It is useful to present a good 1D-Var retrieval initially in order to highlight how the problematic cases differ. Figure 4.3 can be considered a good case, converging in 19 iterations, with a $2J/m$ = 0.38. In the upper left panel we show profiles of observed $\alpha_1(a)$, $\alpha_2(a)$ and $\alpha_2(a) - \alpha_1(a)$ differences. There is a clear discontinuity in the observations above 500 km because the L1 and L2 measurements are missing and they are set to the missing data indicator. However, the $\alpha_2(a) - \alpha_1(a)$ difference values are 0, which is a valid ionospheric bending angle value. There is also missing data just below 100 km. Otherwise, these curves all display the characteristic "Z" shape of the ionospheric bending angle profile described in Culverwell and Healy (2015), which can be reproduced with the VaryChap functions. The upper right panel of Figure 4.3 shows $\alpha_2 - (f_1/f_2)^2\alpha_1$ as a function of impact parameter, a. This consistency check is useful for quality control (QC) purposes, because the magnitude of the quantity should be comparable to or smaller than the bending angle uncertainty estimates used in the retrieval (2 microradians) because the ionospheric bending angles scale as $1/f^2$. This condition is clearly met in interval between 100 km to 500 km for this case, where the differences are well below 0.5 microradians. If this is not the case, it indicates that either one or both of the observed bending angle profiles contain large errors. The lower panel left shows the observed $\alpha_2(a) - \alpha_1(a)$ values (green line) and those computed with the 1D-Var solution, $H(\mathbf{x}_a)$ (black line). The 1D-Var solution is able to fit the observations closely, consistent with the reasonable cost at convergence value. It should be noted again that only measurements in the interval between 150 km and 500 km influence the 1D-Var solution, but it is interesting to see how well the 1D-Var solution can predict the observed $\alpha_2(a) - \alpha_1(a)$ values outside this interval. In this case, the 1D-Var solution, $H(\mathbf{x}_a)$, provides a good estimate of the bending angle differences above 500 km and below 150 km when they are available (lower left panel) giving some confidence in the method. The retrieved electron density is shown in the lower right panel, with the electron density having peak value of $3 \times 10^{11}\mathrm{m}^{-3}$ at 300 km and a profile that looks physically reasonable.

Figure 4.4 shows the retrieval with the largest cost at convergence ($2J/m$ =882.5) identified in Figure 4.1. In this case, the retrieval fails because the observation errors are large when compared with the 2 microradian uncertainty assumed in the $\mathbf{R}$ matrix. The L2 bending angles have gross errors below 400 km (see blue line, top left panel) resulting in poor quality bending angle differences used in the 1D-Var. This problem is also clearly evident in the $\alpha_2 - (f_1/f_2)^2\alpha_1$ consistency check, with values greater than 200 microradians below 400 km. Overall, this case should be screened out in the retrieval QC step because the observation information is poor, and it highlights the value of both the $2J/m$ and $\alpha_2 - (f_1/f_2)^2\alpha_1$ diagnostics for this purpose.

Figure 4.5 illustrates a more subtle problem than Figure 4.4, where the L2 signal is poor over a relatively narrow vertical interval. We can use the $\alpha_2 - (f_1/f_2)^2\alpha_1$ to remove around 10 $\%$ of the erroneous bending angles in the 300 km to 400 km interval, by giving them 0 weight in the 1D-Var

retrieval when the magnitude of this difference is greater than 10 microradians. This modification reduces the $2J/m$ value from 33 when all data is used to 0.41, and it is simple to implement in ROPP. In some cases, both the L1 and L2 bending angles are missing, but as noted above the $\alpha_2 - \alpha_1$=0 is treated as a valid value and used in the 1D-Var, as illustrated in Figure 4.6, where the data is missing above 400 km but the 1D-Var solution tries to fit it. It is relatively simple to modify ROPP to remove observations from the 1D-Var (give zero weight) if either of the L1 or L2 bending angles are flagged as missing. However, the question then arises how of many of the 351 bending angles can be missing before the entire retrieval should be flagged as suspicious. For example, we find that 53 profiles have more than 10 % either missing or with $\alpha_2 - (f_1/f_2)^2\alpha_1$ differences greater than 10 microradians in the 150 km to 500 km interval. Not all of these cases produce a large $2J/m$, so this "percentage of bending angles used" check is a potentially useful additional QC diagnostic.

Given that only bending angles in the vertical interval between 150 km to 500 km are actively assimilated in the 1D-Var, it seems reasonable to expect the VarChap layers to peak within this interval. However, in Figure 4.7 this is not the case, with one layer peaking well below 100 km. The 1D-Var solution is a good fit to the observed bending profile, and neither the $2J/m$ value nor the number of iterations (it=19) are problematic. The unphysical retrieval seems to be caused by the negative $\alpha_2 - \alpha_1$ differences below 200 km. Cases like this can be identified by checking the peak heights of the VaryChap layers (r_m). It is found that 103 cases have heights below 150 km, but this number drops to 26 below 120 km and just 8 cases below 100 km. The $2J/m$ value only appears to identify about 10 % of the cases where the peak height is below 150 km. In contrast, only 8 cases have a layer peaking above 500 km, but 5 of these are flagged by the $2J/m$ test. Given the number of cases where the peak height is outside the assimilation interval (150 - 500 km), checking the heights of the VaryChap layers appears to be a useful test.

There are 94 cases where $2J/m$ < 0.1, of which 59 cases can be considered low electron density cases, defined here as a maximum electron density in the profile less than $5 \times 10^{10}\mathrm{m}^{-3}$. Figure 4.8 is one example of a low electron density case, with a peak electron density below $1.5 \times 10^{10}\mathrm{m}^{-3}$ and a $2J/m$ value of 0.039. The problem with this retrieval is that the magnitude of the largest $\alpha_2 - \alpha_1$ bending angle differences is below the assumed uncertainty value which is 2 microradians. This assumed uncertainty value was found by trial and error in Healy and Culverwell (2021), but these GRAS extension results suggest it is not appropriate for the low electron density cases. One approach that could be tested in future work is to scale by uncertainty value by the maximum $(\alpha_2 - \alpha_1)$ difference.

Single Frequency Retrievals

The largest $2J/m$ value shown in Figure 4.4 is a case where the L2 observations are poor, but the L1 observations appear to be reasonable. Therefore, it is natural to investigate if the retrieval can be performed using single frequency observations. The ROPP source code can be adapted quite easily to process single frequency retrievals (see Appendix). This is because the bending angle forward operator, Eq. 2.5, is composed of a frequency dependent term, multiplied by a term that depends on the ionospheric state. The use of a single frequency assumes that the neutral bending angle is negligible above 150 km, and that $\alpha_2 - \alpha_1$ differencing is not required to correct for the neutral bending. The forward model can be modified to compute just the L1 bending angles by changing the frequency dependent term, and Eq. 2.5 becomes

$$\alpha_1(a) = \frac{k_4}{f_1^2}\left[a\left[\int_a^{r_L} + \int_a^{r_G}\right]\frac{\frac{dn_e(r)}{dr}}{\sqrt{(r^2-a^2)}}dr - \frac{n_e(r_L)a}{\sqrt{(r_L^2-a^2)}}\right]. \tag{4.1}$$

The observation vector, $\mathbf{y}$, is populated with the L1 bending angles, $\alpha_1(a)$. Figure 4.9 reproduces Figure 4.4 but using just the L1 bending angles in the 1D-Var. The $2J/m$ reduces from 882 to 0.16

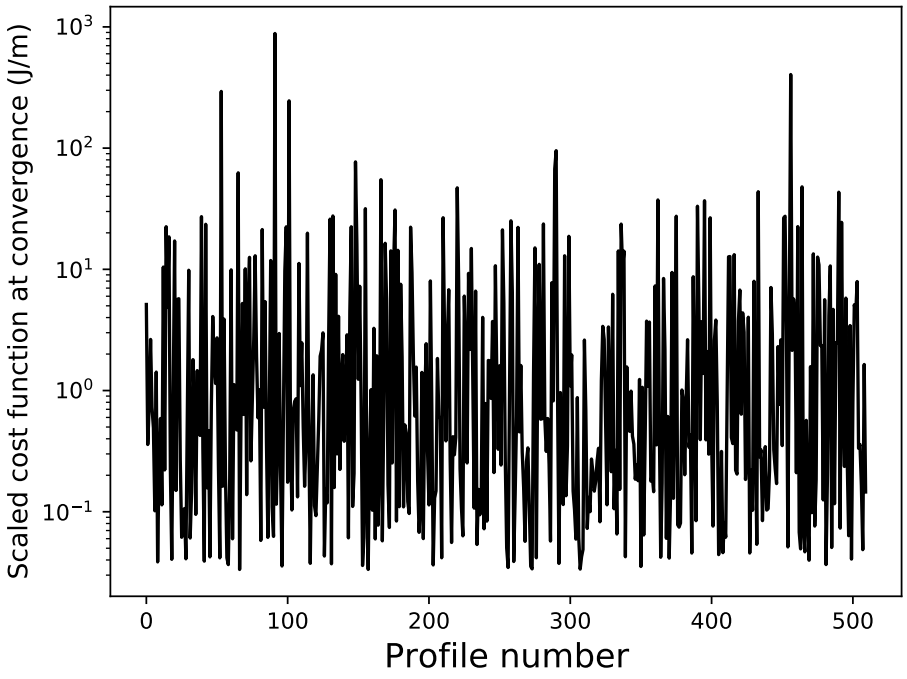

Figure 4.1: The cost at convergence values for the Metop extension retrievals on August 1, 2020.

and the solution converges in 19 iterations. More generally, the full data set has been processed using just the L1 bending angles. The mean $2J/m$ is 10.4 and the mean number of iterations is 21.4 which is greater than the mean number of 19 iterations required for the $\alpha_2 - \alpha_1$ retrievals. In addition, around 10 % of the retrievals fail as a result of passing missing L1 data to the 1D-Var. As shown earlier (Figure 4.6), missing data appears to be less problematic in the dual frequency retrievals if both the L1 and L2 bending angles are missing, because $\alpha_2 - \alpha_1$=0 is interpreted is a valid ionospheric bending angle. However, these bending angle differences should not be used because they produce erroneous dual frequency retrieval results. The more obvious missing L1 data problem can be solved for the single frequency implementation with better QC in the preprocessing steps.

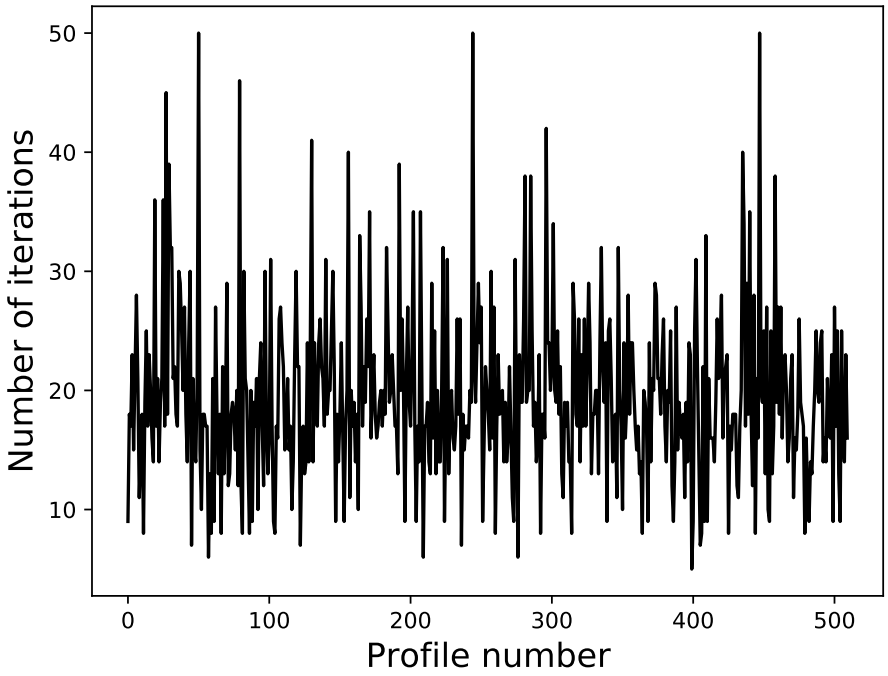

Figure 4.2: The number of 1D-Var iterations required for convergence for the Metop extension data. The retrieval exits after 50 iterations.

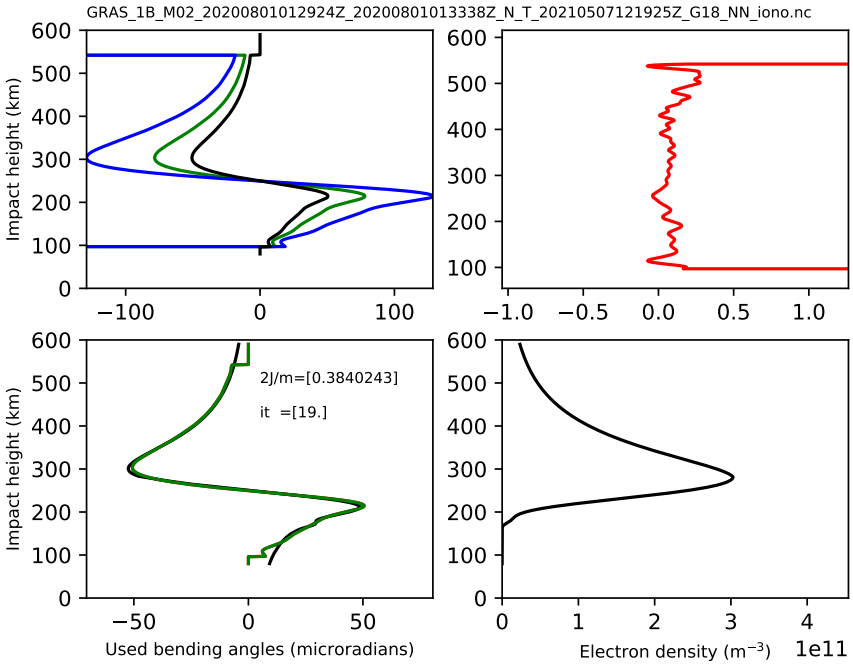

Figure 4.3: A "good" retrieval. Upper left: The $\alpha_2(a)$ (blue), $\alpha_1(a)$ (green) and $(\alpha_2(a) - \alpha_1(a))$ (black) bending angle profiles. Upper right: $(\alpha_2 - (f_1/f_2)^2\alpha_1)$ as a function of impact parameter (height). Lower left: Observed $\alpha_2(a) - \alpha_1(a)$ differences (green) and those given by $H(\mathbf{x})$ using the 1D-Var solution (black). Lower right: the retrieved electron density profile. All bending angles are given in microradians. The measurement identifier is given in the title.

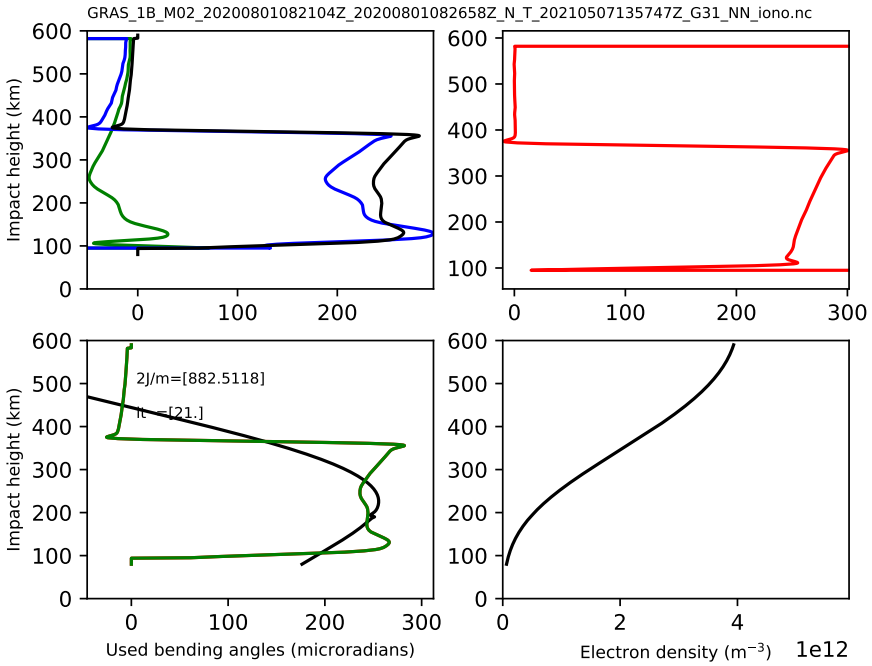

Figure 4.4: As Figure 4.3 but showing the retrieval with the largest cost at convergence in the dataset.

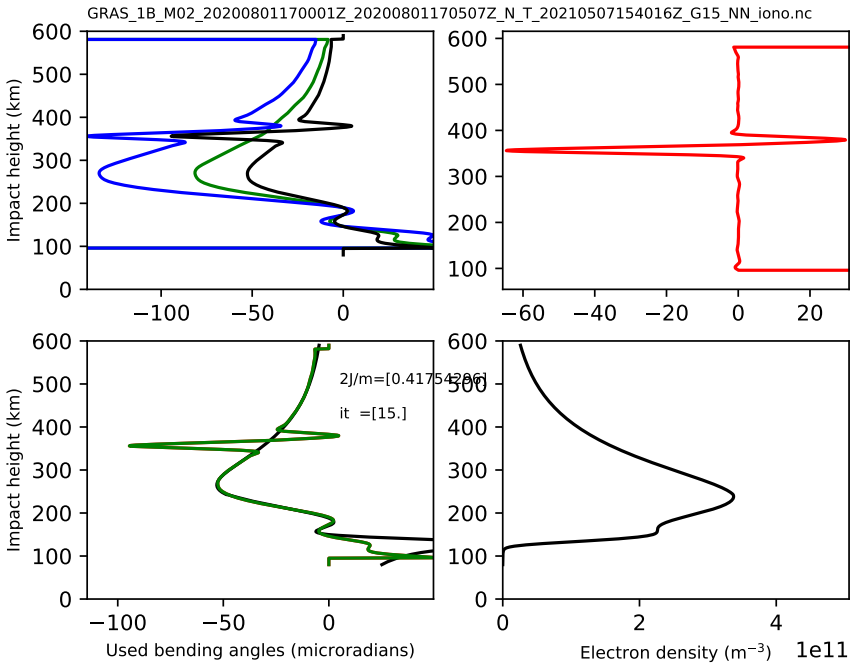

Figure 4.5: As Figure 4.3 but with the problematic bending angle differences in 300 km to 400 km interval, identified using $\alpha_2 - (f_1/f_2)^2\alpha_1$ differences.

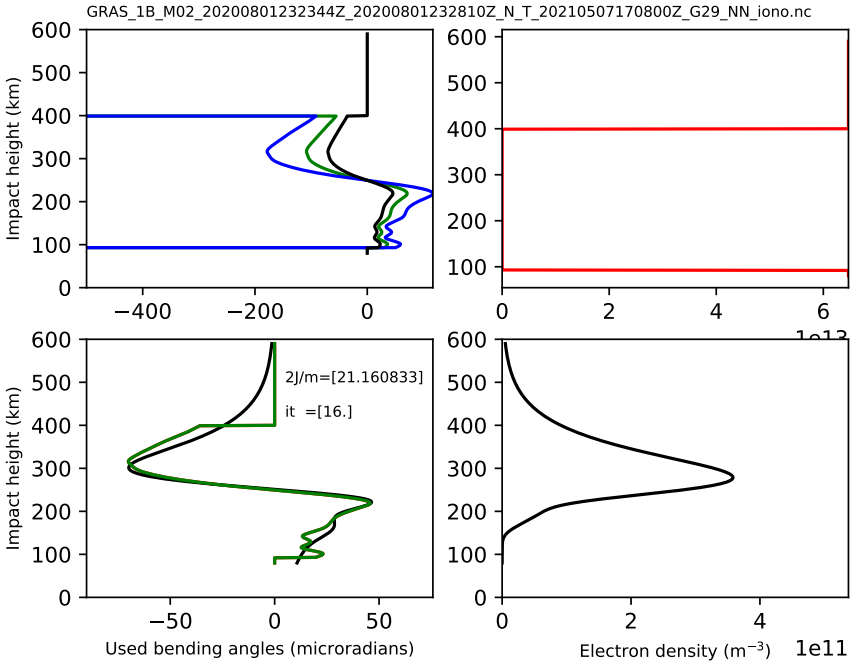

Figure 4.6: As Figure 4.3 but showing a retrieval where a significant number of both L1 and L2 bending angles are missing above 400 km.

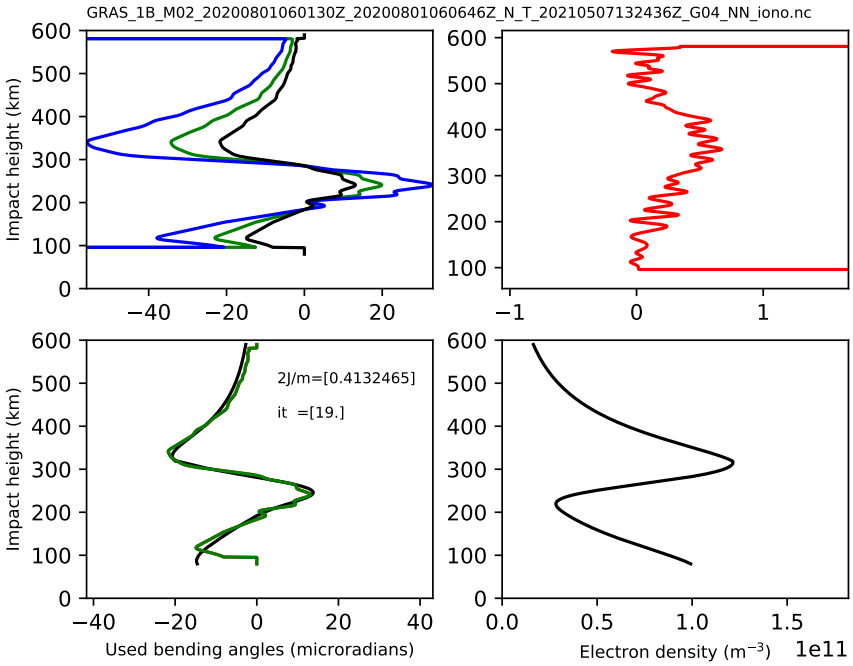

Figure 4.7: As Figure 4.3 but showing a retrieval where the peak of the lower VaryChap level is below 100 km.

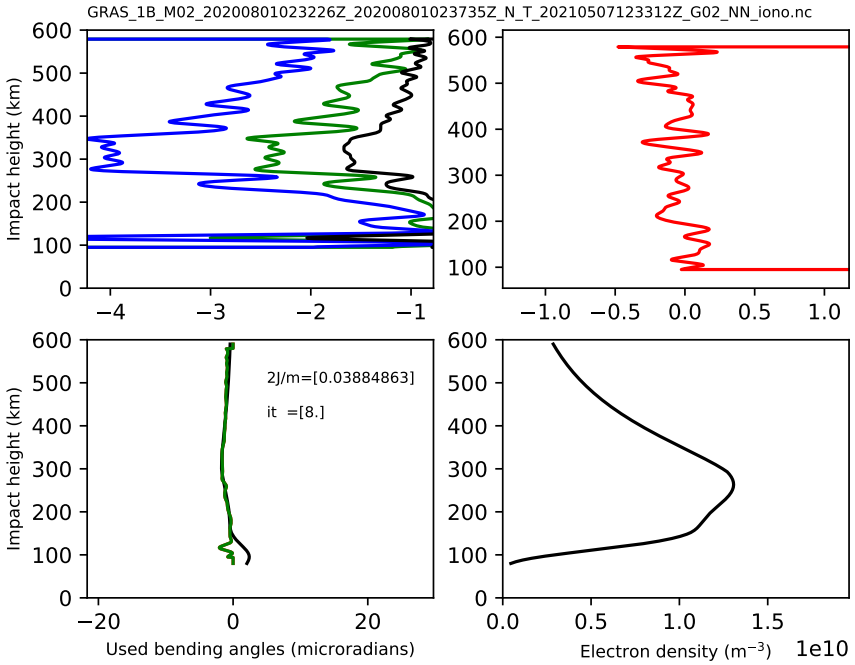

Figure 4.8: As Figure 4.3 but showing a low electron density retrieval where the $2J/m$ value is low.

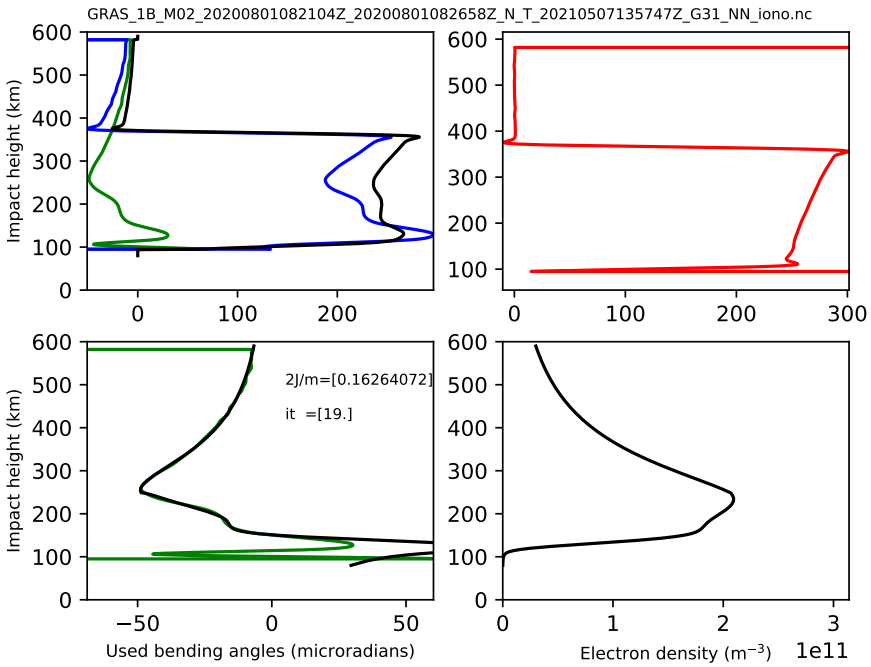

Figure 4.9: As Figure 4.4, but showing the electron density retrieval using just the L1 bending angles.

5 Summary

We have successfully processed a Metop GRAS extension dataset that provides bending angles up to 600 km using the ROPP-11 ionospheric 1D-Var retrieval code. These 1D-Var retrievals are based on two VaryChap layers, and the $(\alpha_2 - \alpha_1)$ bending angle differences are given on a 1 km vertical grid. They are used (actively assimilated) in the 1D-Var between 150 km and 500 km in the vertical, and the observation uncertainty is assumed to be 2 microradians.

Around 15 % of the 510 profiles either converge to a high $2J/m$ "cost at convergence" value or fail to converge in 50 iterations. Visual inspection of the retrieval output has revealed that in many cases either that a significant number of bending angles are missing in the 150 km to 500 km interval, or the α_1 and α_2 are not "consistent", meaning that the $\alpha_2 - (f_1/f_2)^2\alpha_1$ differences are large compared to the 2 microradian uncertainty value used in the observation uncertainty matrix, $\mathbf{R}$. Additional quality control (QC) can be used to identify the missing data and when the L1 and L2 bending angles are not consistent, so that they are given no weight when determining the 1D-Var solution. This additional QC should be introduced into ROPP-12. However, this step can still lead to poor quality retrievals if too many observations are given zero weight. Therefore some monitoring of the percentage of bending angles used in the 1D-Var is useful. For example, in this study we found that when these additional QC checks are used 53 profiles have more than 10 % of the bending angles given no weight in the minimization. This "percentage used" information is also useful for QC.

Some problematic retrievals are not identified with either the $2J/m$ check or the iteration number. In particular, we are finding cases where a VaryChap peak height, r_m, is too low. It may be possible to adapt the retrieval code to stop these unphysical retrievals, but we currently recommend that the 1D-Var solution r_m values are checked prior to use.

Overall, the we suggest the following QC checks should be considered when assessing the quality of the 1D-Var retrievals:

- large cost at convergence: $2J/m$ > 10
- failure to converge: it=50
- percentage of bending angle "used" in the 150 - 500 km vertical interval. Flag if less than 90 %
- 1D-Var solution VaryChap peak heights (r_m) below 100 km

It is found that the assumed 2 microradian bending angle uncertainty is probably not appropriate for low electron density cases where the magnitude of the $\alpha_2 - \alpha_1$ differences can be around 2 microradians. This suggests that more flexible $\mathbf{R}$ should be investigated in the future. Finally, it is relatively easy to adapt the 1D-Var source code to process single frequency bending angles, rather than bending angle differences (see Appendix). It is demonstrated that this can solve some problems associated with poor L2 bending angles. However, it needs to be implemented alongside the improved QC, to screen out missing bending angle data more effectively. The single frequency retrieval approach assumes that the neutral bending can be neglected for impact parameters above 150 km. If this neutral bending assumption is valid, then a retrieval based on the sum $(\alpha_2 + \alpha_1)$ as a function of impact parameter should also work, and this new observation vector may have better noise characteristics. This could also be investigated in future work.

Appendix: Code changes for single frequency processing

It is straightforward to modify the existing ionospheric 1D-Var code to use a single frequency, for example L1. In the main program, `ropp_1dvar_dbangle.F90`, we change the code to populate the observation vector with the L1 bending angles instead of the L2-L1 bending angle differences (commented out below):

```
!-------------------------------------------------------------------------------
! 10. Read observation data and covariance matrix
!-------------------------------------------------------------------------------

    CALL message(msg_info, &
                 "Reading observation data for profile " // TRIM(istr) // &
                 " from the file\n      " // TRIM(config % obs_file) // ".\n")

    CALL ropp_io_read(obs_data, config%obs_file, rec=i, ranchk=ranchk)

    obs%diff_bangle = .TRUE.  ! To get roprof2obs to infer r_gns and r_leo.

! Remove
!    obs_data%Lev1b%bangle = obs_data%Lev1b%bangle_L2 - obs_data%Lev1b%bangle_L1

! Add
    obs_data%Lev1b%bangle = obs_data%Lev1b%bangle_L1
```

In the both forward operator and tangent linear code

- `ropp_fm_dbangle_1d.f90`
- `ropp_fm_dbangle_1d_tl.f90`

we change the frequency dependent constant to k_4/f_1^2 to be consistent with Eq.4.1

```
!
!  iono_const = k4 * (f1 - f2) * (f1 + f2) / (f1*f2)**2
!
  iono_const = k4 / f1**2
```

but otherwise the main calculation remains the same.

References

Culverwell, I. D., and S. B. Healy, 2015: Simulation of L1 and L2 bending angles with a model ionosphere. *ROM SAF Report*, **17**, https://www.romsaf.org/rsr.php.

Elvidge, S., 2021: Ionospheric 1D-Var Retrieval Assessment. *ROM SAF Visiting Scientist Report*, **39**, https://www.romsaf.org/visiting_scientist.php.

Healy, S. B., and I. D. Culverwell, 2021: A one-dimensional variational retrieval for truncated GNSS radio occulation measurements. *ROM SAF Report*, **42**, https://www.romsaf.org/rsr.php.

Hoque, M. M., F. S. Prol, M. Henandez-Pajares, R. Notarpieto, L. Yuan, G. Oliveras-Pulido, V. Graffigna, A. V. Engeln, and C. Marquardt, 2023: Assessment of GRAS Ionospheric Measurements for ionospheric model assimilation. *Remote Sensing*, Submitted.

Nsumei, P., B. W. Reinisch, X. Huang, and D. Bilitza, 2012: New Vary-Chap profile of the topside ionosphere electron density distribution for use with the IRI model and the GIRO real time data. *Radio Science*, **47**, 4, doi.org/10.1029/2012RS004989.

Rodgers, C. D., 2000: *Inverse methods for atmospheric sounding: Theory and practice*. World Scientific Publishing, Singapore, New Jersey, London, Hong Kong.

ROM SAF (and earlier GRAS SAF) Reports

SAF/GRAS/METO/REP/GSR/001	Mono-dimensional thinning for GPS Radio Occulation
SAF/GRAS/METO/REP/GSR/002	Geodesy calculations in ROPP
SAF/GRAS/METO/REP/GSR/003	ROPP minimiser - minROPP
SAF/GRAS/METO/REP/GSR/004	Error function calculation in ROPP
SAF/GRAS/METO/REP/GSR/005	Refractivity calculations in ROPP
SAF/GRAS/METO/REP/GSR/006	Levenberg-Marquardt minimisation in ROPP
SAF/GRAS/METO/REP/GSR/007	Abel integral calculations in ROPP
SAF/GRAS/METO/REP/GSR/008	ROPP thinner algorithm
SAF/GRAS/METO/REP/GSR/009	Refractivity coefficients used in the assimilation of GPS radio occultation measurements
SAF/GRAS/METO/REP/GSR/010	Latitudinal Binning and Area-Weighted Averaging of Irregularly Distributed Radio Occultation Data
SAF/GRAS/METO/REP/GSR/011	ROPP 1dVar validation
SAF/GRAS/METO/REP/GSR/012	Assimilation of Global Positioning System Radio Occultation Data in the ECMWF ERA-Interim Re-analysis
SAF/GRAS/METO/REP/GSR/013	ROPP PP validation
SAF/ROM/METO/REP/RSR/014	A review of the geodesy calculations in ROPP
SAF/ROM/METO/REP/RSR/015	Improvements to the ROPP refractivity and bending angle operators
SAF/ROM/METO/REP/RSR/016	Simplifying EGM96 undulation calculations in ROPP
SAF/ROM/METO/REP/RSR/017	Simulation of L1 and L2 bending angles with a model ionosphere
SAF/ROM/METO/REP/RSR/018	Single Frequency Radio Occultation Retrievals: Impact on Numerical Weather Prediction
SAF/ROM/METO/REP/RSR/019	Implementation of the ROPP two-dimensional bending angle observation operator in an NWP system
SAF/ROM/METO/REP/RSR/020	Interpolation artefact in ECMWF monthly standard deviation plots
SAF/ROM/METO/REP/RSR/021	5th ROM SAF User Workshop on Applications of GPS radio occultation measurements
SAF/ROM/METO/REP/RSR/022	The use of the GPS radio occultation reflection flag for NWP applications
SAF/ROM/METO/REP/RSR/023	Assessment of a potential reflection flag product
SAF/ROM/METO/REP/RSR/024	The calculation of planetary boundary layer heights in ROPP
SAF/ROM/METO/REP/RSR/025	Survey on user requirements for potential ionospheric products from EPS-SG radio occultation measurements

ROM SAF (and earlier GRAS SAF) Reports (cont.)

SAF/ROM/METO/REP/RSR/026	Estimates of GNSS radio occultation bending angle and refractivity error statistics
SAF/ROM/METO/REP/RSR/027	Recent forecast impact experiments with GPS radio occultation measurements
SAF/ROM/METO/REP/RSR/028	Description of wave optics modelling in ROPP-9 and suggested improvements for ROPP-9.1
SAF/ROM/METO/REP/RSR/029	Testing reprocessed GPS radio occultation datasets in a reanalysis system
SAF/ROM/METO/REP/RSR/030	A first look at the feasibility of assimilating single and dual frequency bending angles
SAF/ROM/METO/REP/RSR/031	Sensitivity of some RO measurements to the shape of the ionospheric electron density profile
SAF/ROM/METO/REP/RSR/032	An initial assessment of the quality of RO data from KOMPSAT-5
SAF/ROM/METO/REP/RSR/033	Some science changes in ROPP-9.1
SAF/ROM/METO/REP/RSR/034	An initial assessment of the quality of RO data from Metop-C
SAF/ROM/METO/REP/RSR/035	An initial assessment of the quality of RO data from FY-3D
SAF/ROM/METO/REP/RSR/036	An initial assessment of the quality of RO data from PAZ
SAF/ROM/METO/REP/RSR/037	6th ROM SAF User Workshop
SAF/ROM/METO/REP/RSR/038	An initial assessment of the quality of RO data from COSMIC-2
SAF/ROM/METO/REP/RSR/039	Impacts of RO mission differences on trends in multi-mission data records
SAF/ROM/METO/REP/RSR/040	Anomalous GRAS radio occultations
SAF/ROM/METO/REP/RSR/041	Assessment of sensitivity of the ROM SAF 1D-Var solutions to various error covariance choices
SAF/ROM/METO/REP/RSR/042	A one-dimensional variational retrieval for truncated GNSS radio occulation measurements

ROM SAF Reports are accessible via the ROM SAF website: https://rom-saf.eumetsat.int